AGU ADVANCING EARTH AND SPACE SCIENCE

Water Resources Research

RESEARCH ARTICLE
10.1029/2020WR027070

Key Points:
- Sparse vegetation has a significant effect on forested floodplain fluid retention at low flows but at the high flows become negligible
- As discharge increases on forested floodplains, fluid retention declines toward the same value regardless of vegetation composition
- As vegetation density increases, lateral mixing becomes increasingly more dominant (relative to longitudinal) than for less dense cases

Supporting Information:
- Supporting Information S1

Correspondence to:
P. A. Carling,
p.a.carling@soton.ac.uk

Citation:
Carling, P. A., Leyland, J., Kleinhans, M. G., Besozzi, L., Duranton, P., & Trieu, H., et al. (2020). Quantifying fluid retention due to natural vegetation in a forest floodplain analogue using the aggregated dead zone (ADZ) dilution approach. *Water Resources Research*, *56*, e2020WR027070. https://doi.org/10.1029/2020WR027070

Received 8 JAN 2020
Accepted 19 JUN 2020
Accepted article online 22 JUN 2020

Quantifying Fluid Retention Due to Natural Vegetation in a Forest Floodplain Analogue Using the Aggregated Dead Zone (ADZ) Dilution Approach

Paul A. Carling[1], Julian Leyland[1], Maarten G. Kleinhans[2], Louison Besozzi[3], Pierre Duranton[3], Hai Trieu[1], and Roy Teske[2]

[1]School of Geography and Environmental Science, University of Southampton, Southampton, UK, [2]Faculty of Geosciences, Physical Geography, Universiteit Utrecht, Utrecht, The Netherlands, [3]Centre d'Enseignement et de Rescherche de Paris, Élève à l'Ecole des Arts et Métiers ParisTech, Paris, France

Abstract Fluid retention and flow resistance due to natural vegetation remain poorly understood despite the importance of understanding these for flow routing and floodplain revegetation projects. Experiments were undertaken in a shallow earthen channel containing a natural cover of small trees, herbaceous plants, and leaf litter, which were sequentially removed and subjected to a range of flows. A dilution monitoring approach within the Aggregated Dead Zone framework was applied to a series of floodplain vegetated flows, yielding information on bulk flow parameters including tracer dispersion, fluid retention, and flow resistance at the reach scale. The primary response of flow to vegetation removal was a small increase in bulk velocity, with depth and wetted width decreasing only slightly. Reach mean travel time and the advective time delay decreased by about a factor of 2 with the removal of herbs, grass, and leaf litter, leaving only trees. Removing the trees, leaving a bare earthen channel, only slightly decreased travel times. Flow resistance and retention exhibited large values for low discharge and converged on a constant low value for relatively high discharges. It is concluded that flow resistance during low flow is higher than in a high flow with the same vegetation. Consequently, sparse vegetation has a prominent effect on hydraulic retention compared with an unvegetated channel at low discharges but this becomes negligible during high discharges as momentum increasingly dominates the flow. This outcome casts doubt on the efficacy of scrubby vegetation to impede higher-velocity floodplain flows, showing need for field-scale determination of integral floodplain resistance.

1. Introduction

Despite significant work, there is still a lack of scientifically robust practical methods that can be applied to natural riparian and floodplain vegetation to explain its role in moderating flow resistance of overbank river flows (Rhee et al., 2008). The issue is relevant to understanding how river planform develops (Braudrick et al., 2009; Gurnell et al., 2012; Tal & Paola, 2007; van Dijk et al., 2013), in determining reforestation strategies for floodplains and wetland management and in flood routing (Tealdi et al., 2010). Emergent vegetation has environmental and recreational value in riparian and floodplain areas where it may control large woody-debris production whilst the submerged portions mediate flow resistance and sediment transport (Dittrich & Järvelä, 2005; Fathi-Maghadam & Kouwen, 1997; Jeffries et al., 2003; Li & Shen, 1973; Pasche & Rouvé, 1985). Due to enhanced resistance, a vegetated floodplain can cause flood attenuation, lowering flood peaks but extending the period of high water. Thus, at upstream forested locations, deeper and more extensive floodplain flooding can be prolonged, but in contrast, downstream locations may benefit from the resulting flood attenuation (Darby, 1999).

Regardless of the highly complex physical configuration of natural floodplain vegetation (Ishikawa et al., 2000), it is usual to consider a flooded vegetated surface conceptually as either submerged or emergent, depending on whether the vegetation protrudes above the water surface. Furthermore, flow modeling commonly depends on vegetation characterization in the form of patches with constant flow resistance independent of flow discharge, which is sensitive to uncertainty in mapped land cover and attributed flow resistance (Straatsma et al., 2013). In addition, the vertical flow structure can be divided into "unobstructed flow" (for that portion of the flow that is above fully submerged vegetation) and "obstructed flow" (for flow through

submerged vegetation) (Aberle & Järvelä, 2013). A consideration of the near-bed flow layer might usefully also address the "soil-bed roughness" (Huai et al., 2009). This simple tripartite scheme is complicated when the vegetation consists of an understory and a canopy consisting of different vegetative roughness elements (Hui et al., 2010; Järvelä, 2002). Thus, the understory can be submerged when the canopy is emergent. Such a situation is common when a natural flooded forest is considered, as trees usually have an understory of herbaceous plants and grasses with a groundcover of leaf litter. The usual controlled laboratory experiments largely pertain to rigid or (less-commonly) flexible in-channel vegetation and rarely reproduce well the complexity of natural floodplain situations and so novel solutions might be useful. Although the literature concerning fluid retention by flooded vegetation often considers the complex distortion of velocity profiles within arrays of vegetative elements at singular points in flumes (Li et al., 2013; Shucksmith et al., 2011) and the flow resistance due to grouped elements (e.g., Kothyari et al., 2009; Nepf, 1999a; Schoneboom et al., 2011), there is an overriding interest in the fluid retention due to bulk characteristics of the vegetation at the reach scale not least for practical applications. Moreover the data required for complex theoretical analyses frequently are difficult to obtain (Aberle & Järvelä, 2013) and often recourse is made to consideration of plants as simple vertical cylinders (e.g., Bennett et al., 2002; Ghisalberti & Nepf, 2005; Nepf, 1999b) with modeling utilizing arbitrary drag coefficients (Järvelä, 2004). Rather, there is a requirement for quantified examples of bulk flow retardation by natural vegetation in natural settings from which data might be used to improve the development of generic theory-based methodologies.

The approach herein uses a proven solute tracer method to determine bulk flow characteristics of open channels and applies it to the flow through a naturally vegetated shallow experimental channel. Although solute dilution has been widely used for river gauging and determining open-channel mixing processes (Fukuoka & Sayre, 1973; Valentine & Wood, 1977), the approach has not been developed widely with respect to fluid retention by natural vegetation in the field (Serra et al., 2004) and with only limited application in flume studies (Ghisalberti & Nepf, 2005; Hamidifar et al., 2015; Nepf, 1999b; Nepf et al., 1997; Perucca et al., 2009; Shucksmith et al., 2011). Specifically, Aberle and Järvelä (2013) and Curran and Hession (2013) make no mention of dilution techniques in their methodological reviews. However, reach-scale dispersion modeling has considerable potential not offered by point measurements within flow as it quantifies the reach-scale bulk effects of vegetation rather than the highly localized effects of individual plant elements. The aggregated dead zone (ADZ) model (Beer & Young, 1983), in particular, provides a framework to explore bulk effects of fluid dispersion which is particularly useful in cases of complex flow geometries wherein there is significant fluid retention (Beven & Carling, 1992; Boxall et al., 2003; Green et al., 1994; Guymer & O'Brien, 2000; Wallis et al., 1989, 1990; Wallis, 1994). Application of a dilution technique considers flow in bulk and so there can be no treatment of complex velocity profiles or individual point velocities. Rather the longitudinal mixing conceptually is due to a combination of longitudinal shear dispersion and transverse diffusion and mixing such that with flow partitioning around multiple plant stems, fluid retention occurs at the bulk flow scale as well as at the scale of the individual stem. Although for dense submerged vegetation a complex coupled vertical velocity profile may develop between the free flow and the flow within the vegetation canopy as noted above, in the case of relatively sparse vegetation in shallow flow at low channel gradient as described below, shear velocities are small (Rutherford, 1994). In the latter case, the vertical velocity structure remains well mixed such that a boundary-layer extends throughout much of the depth (Shucksmith et al., 2011), longitudinal dispersion coefficients are comparatively low (Murphy et al., 2007) and bulk flow parameters can be deduced without recourse to analysis of vertical flow structure. Thus, an important concept underlying the current analysis is that the balance between longitudinal mixing (K_t) and transverse mixing (K_m) is moderated by the presence of vegetation which tends to enhance transverse mixing at the expense of longitudinal mixing (Shucksmith et al., 2011). This concept is shown schematically in Figure 1 and underlies the approach to the discussion. In Figure 1a, the flow is well mixed in the vertical but displays poor transverse mixing whereas, in contrast, in Figure 1b transverse mixing is enhanced by denser vegetation.

Floodplains are never completely flat but are characterized by linked shallow linear depressions that are important for conveyance of both water and sediment (Lewin et al., 2016). This paper considers an analogue for a shallow flooded forest floodplain depression, to elucidate how effective scattered tree cover with an understorey of herbs is in retarding floodplain flow, and what the contributions of these components of vegetation are to the overall retardation and flow resistance. Whilst controlled experiments usually demonstrate that the presence of vegetation increases fluid retention in contrast to bare earth, the actual increment is

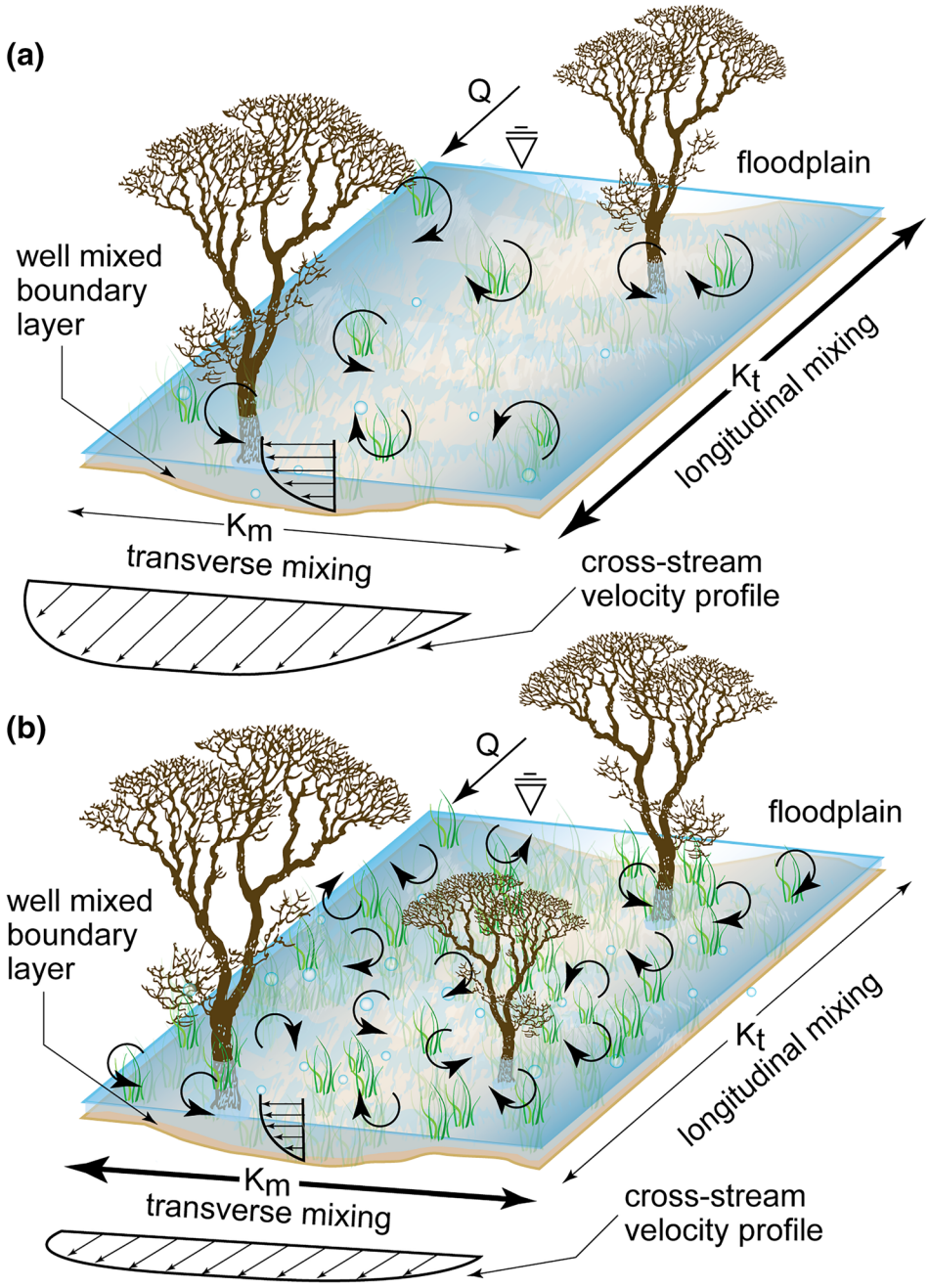

Figure 1. Conceptualization of the role of submerged vegetation in moderating the balance between longitudinal mixing (K_t) and transverse mixing (K_m). (a) Sparse vegetation: K_t dominates K_m. (b) Dense vegetation: The dominance of K_t over K_m is reduced. The presence of vegetation tends to enhance transverse mixing at the expense of longitudinal mixing. The mathematical definition of K is considered later in the text.

dependent on the vegetation density and the Reynolds number of the flow (Järvelä, 2002). However, model tests of large-scale wetlands have cast doubt on the effectiveness of selective vegetation removal in influencing bulk flow parameters (Paudel et al., 2013). Thus, as a hypothesis, it can be reasonably expected that flow retardation will be high for low Reynolds number discharges and retardation should decline as vegetation is removed. However, in particular, the effect on flow resistance of progressively removing vegetation, contrasting both low-discharge and high-discharge flows, finally to leave a bare earth channel has not been explored previously in a seminatural channel. Therefore, the main objective of

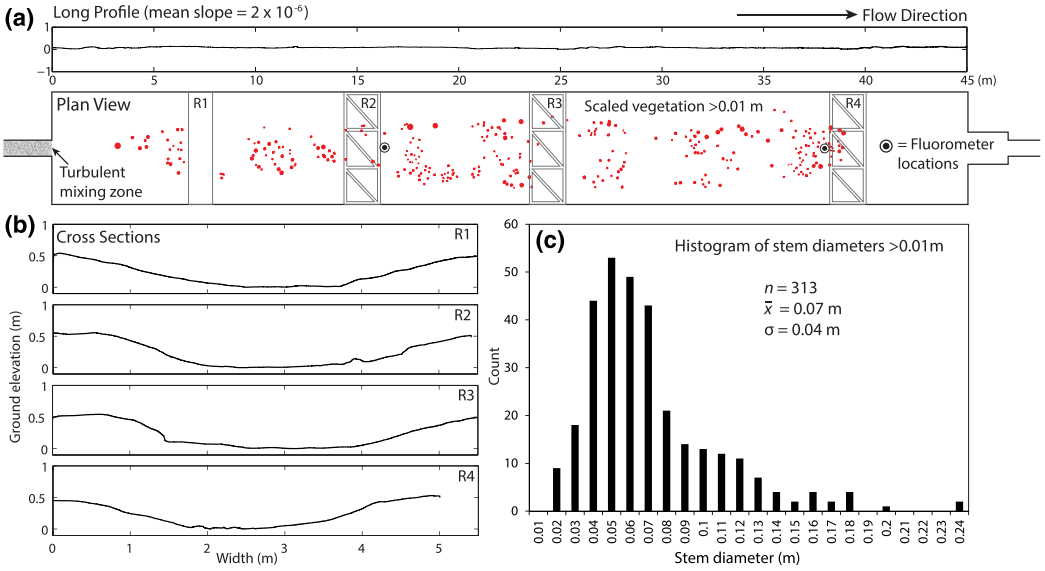

Figure 2. (a) Plan view of experimental facility showing longitudinal profile in center of channel. Red dots represent tree stem diameters drawn to scale. (b) Cross sections at each of the bridge locations. (c) Histogram of stem diameters for 313 trees with stem diameters greater than 0.01 m.

the study is to quantify the variation in bulk fluid retention of different vegetative states within a floodplain forest (consisting of a submergible understory and an emergent canopy) as a function of varying discharge. This objective will be achieved through (1) an experimental design which employs a systematic removal of vegetation to allow the comparison of (a) all vegetation to (b) trees only and (c) bare earth; (2) each vegetation treatment will be observed under different flow conditions, allowing (3) bulk flow and resistance properties to be calculated using the ADZ model, ultimately leading to comparative estimates of flow retardation and flow resistance due to trees, herbaceous ground cover and bare earth on an analogue forest floodplain.

2. Methods

2.1. Experimental Facility

The experimental facility is 45 m long and 5 m wide with a nominal depth [Z] in the center of 0.5 m (Figure 2a). The shallow floodplain depression is formed in earth at a nominal gradient of 2×10^{-6} m/m and the section has side-wall angles of approximately 15° (Figure 2b). There is some longitudinal variation in the section and the longitudinal profile which results in slightly nonuniform flow. Although strictly the flow was not uniform, it has been shown that for flow through emergent vegetation in a channel at very low discharges and for near-zero bed gradient the flow can be considered as nearly uniform with zero acceleration (Lee et al., 2004). Although the date of abandonment of the channel is unknown, tree ring counts in 2012 indicate a minimum period of over 20 years. The upstream end of the channel has a concrete rectangular section together with undershot gate. The downstream end of the channel is a similar concrete section with an overshot gate. A large holding tank and pumps supply a maximum discharge of approximately 0.3 $m^3 s^{-1}$. Experiments were conducted in late October 2012 at which time a rank, sparse but evenly distributed groundcover existed of grass and herbaceous plants with occasional briar stems. This ground cover is treated subsequently as if it has a uniform distribution in terms of flow retardation across the channel. The tree cover consisted mainly of birch (*Betula pendula*) unevenly distributed throughout the channel (Figures 2a and 3) with bole diameters between 0.01 and 0.25 m (Figure 2c). The median bole diameter (L_d) averaged 0.05 m and the approximate spacing of the trees (L_s) averaged over the channel area was 0.5 m, although some clumping occurred (Figure 3). Despite clumping, no rapid flow zones were observed in the experiments, and the average spacing of the trees is used in subsequent analyses. The area of the channel occupied by the number (n_t) of 313 trees in total is around 0.62m^2 or < 0.6% of the plan view area

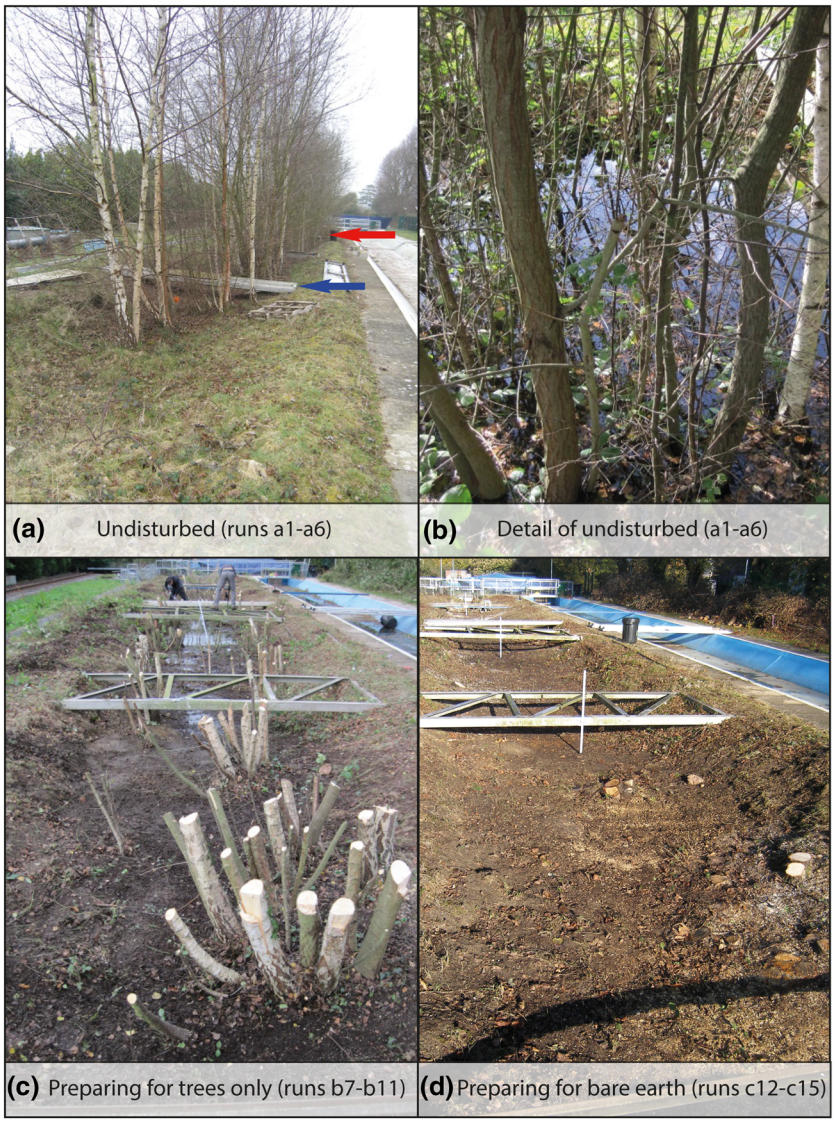

Figure 3. (a) View down the channel. Blue arrow locates the R1 bridge and the red arrow locates the R2 sampling bridge (see also plan view Figure 2a). (b) Side view of emergent trees at R1 with herbaceous plants and litter partially submerged. (c) View down the channel, from R2 toward the bridges at R3 and R4, after the herbaceous and litter layer had been mostly removed. (d) View down the channel, from R2 toward the bridges at R3 and R4, after the removal of trees to leave bare earth.

of the channel. The litter layer was < 0.10 m thick (average dry weight = 1.73 kg m^{-2}; s.d. 0.66 kg m^{-2}; $n = 5 \times 0.5$ m^2 sampled squares) and consisted of well-rotted leaves at depth grading upward to a dry surface leaf cover. Thus, for the whole channel, there was around 360 kg of litter present. Around 1.5 kg of dry litter was flushed out (trapped in a 2.5 mm mesh net downstream of the tailgate) in trials prior to the main experiments and a total of about 3.0 kg washed out during the main experiments. Thus, less than 1% of the litter was lost during the runs and the litter layer remained intact in the first series of experiments.

2.2. ADZ Model for Flow Retardation

The mathematical structure of the ADZ model (Beer & Young, 1983) is outlined by Richardson and Carling (2006) to whom the reader is referred for additional detail, so only a brief introduction is provided

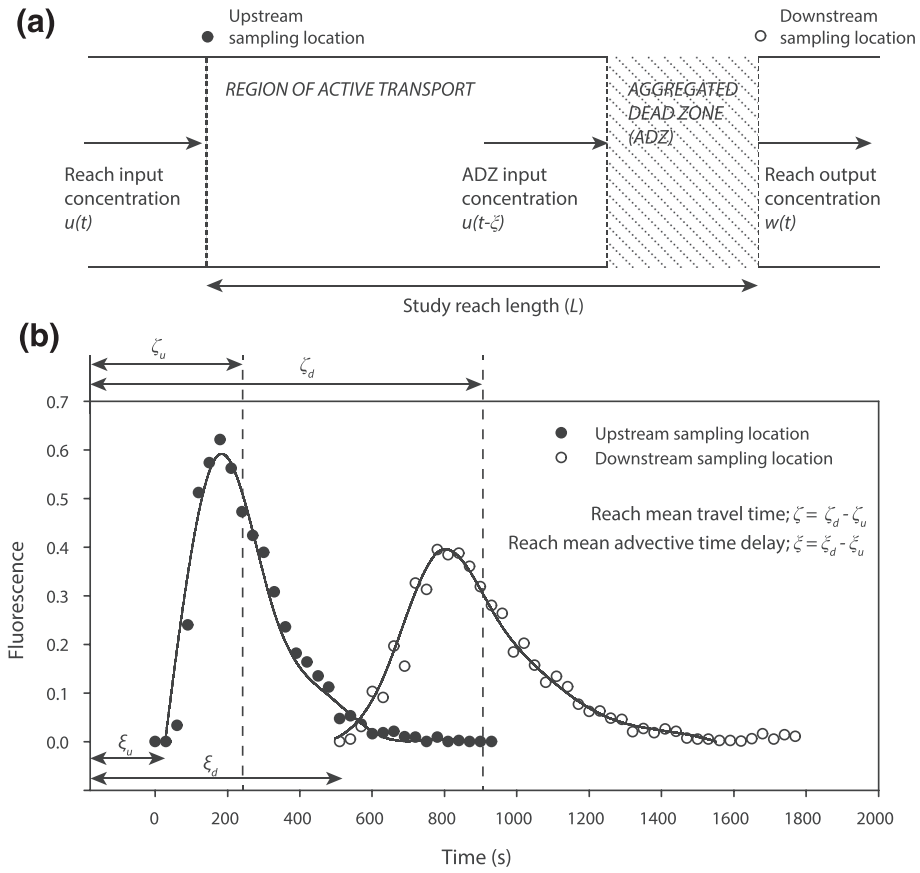

Figure 4. (a) Conceptual representation of a study reach within the ADZ framework. See text for explanation. (b) Definition of basic bulk flow parameters associated with the ADZ model as derived from the fluorescence data sets and spline fits (data shown is from run c13). Modified after Richardson and Carling (2006).

here to the ADZ concept. ADZ models applied to natural vegetation-free channels *conceptually* divide the channel reach into two mixing regions—a central core of moving water and an aggregated dead zone of near-stationary water close to bank line irregularities (Davis et al., 2000). Advection dominates the central core, with little or no longitudinal velocity (U) within the dead zone, although lateral storage and release of tracer occurs from the dead zone. It is important to realize that the concept of an aggregated dead zone does not preclude the actual presence of multiple isolated dead zone areas nor the possibility of other factors delaying flow, such as vegetation. The physical mechanisms of mixing in both regions occur at a variety of scales, from the molecular to large-scale shear-induced turbulence (Davis et al., 2000, p. 360). Relatively large-scale shear flow between the central core and the marginal dead zones contributes significantly to longitudinal mixing, K_t (Davis & Atkinson, 2000). In a vegetated channel, additional shear flows occur around multiple plant stems, as well as modifying the scale of turbulence and introducing additional stem-associated dead zones (Nepf et al., 1997), promoting further lateral mixing, K_m at a section. In this manner, increasing vegetation density influences overall dispersion (Figure 1), and in a well-mixed channel, longitudinal dispersion is dominated by dead zone storage (Beer & Young, 1983; Davis et al., 2000; Wallis et al., 1989). In other studies of vegetative flows, the mixing contribution of turbulence (K_{turb}) is considered in relation to the so-called "mechanical mixing" contribution (K_{mech}) (Serra et al., 2004), which includes shear around plant stems in particular. These parameters are analogous in some degree to K_m and K_t, respectively (Nepf, 1999b), and are introduced here as reference is made to them in the Discussion.

In brief, the ADZ model simply considers the reach output tracer concentration as a function of the reach input concentration and time (Figure 4). To this end, the properties of an upstream and a downstream

Table 1
Experimental Run Scenarios and Flow Conditions

Vegetation condition	Scenario	Flow depth (m)	Discharge (m^3 s^{-1})
a series: Undisturbed natural vegetation of trees (mainly Birch, *Betula pendula*), herbaceous plants, grass, and leaf litter	a1	0.19	0.1
	a2	0.21	0.14
	a3	0.24	0.30
	a4	0.23	0.31
	a5	0.22	0.15
	a6	0.21	0.12
b series: Trees only through removal of herbaceous plants, grass, and leaf litter	b7	0.16	0.05
	b8	0.18	0.02
	b9	0.18	0.03
	b10	0.22	0.06
	b11	0.26	0.11
c series: No vegetation, earth lined flume only after removal of trees	c12	0.22	0.06
	c13	0.24	0.12
	c14	0.18	0.03
	c15	0.18	0.02

Note. Discharge is determined from the dye dilution surveys. The flow depth reported here is the average recorded for each run at station R2.

solute dilution curve at two defined measurement stations are compared for any given experiment. For conservation of solute mass, the area under the downstream concentration curve should agree with that of the upstream curve. For constant discharge (Q), the model assumes a uniform solute concentration within the aggregated dead zone and steady flow such that the volume (V) of the ADZ (defined in Figure 4a and Equation 1) is a constant. Critical parameter values are the first arrival times of the tracer, ξ_u, for the upstream station and ξ_d for the downstream station (Figure 4). The parameter ξ is defined as the time of the first rise in concentration (defined by the curve-fitted procedure: see supporting information) above the background value as the solute plume arrives at the sampling location. Similarly, the respective centroids of the time-concentration curves are as follows: ζ_u and ζ_d (Figure 4), defined by integrating the areas below the curves. The reach mean travel time ($\zeta = \zeta_d - \zeta_u$) is then the difference between the centroid times. Beer and Young (1983) and Richardson and Carling (2006) explain in more detail methods to obtain consistent values of ξ and ζ.

The ADZ residence time (T) is equal to

$$T = (\zeta - \xi) = V/Q \tag{1}$$

where $\xi = \xi_d - \xi_u$ is the advective time delay. The dispersive fraction (D_f), which provides a measure of the dispersive properties of the reach, is defined as follows:

$$D_f = T/\zeta = V/Vr \tag{2}$$

where V_r is the study reach volume defined by the channel shape and water surface. D_f is effectively a normalized parameter, which lumps all the dispersive mechanisms active within the reach as a single discrete volume. Importantly, once basic dilution curve parameters are quantified, and the channel cross-sectional geometry and longitudinal energy slope are known, additional bulk hydraulic data can be calculated, including flood wave celerity, mean flow velocity, Froude and Reynolds numbers, roughness parameters, stress on the channel boundaries, drag coefficients, and dispersion coefficients. These derivations are detailed latterly.

2.3. Experimental Procedure

The first six experiments (a series) considered flow through the undisturbed vegetation (Table 1 and Figure 3a). The herbaceous layer was just fully submerged whilst the tree trunks were partly submersed with the canopies fully emergent. A range of discharges was used from 0.023 to 0.315 m^3 s^{-1} which produced a narrow range of uncontrolled average water depths at R2 from 0.16 to 0.26 m and bulk flow velocities of 0.02 to 0.12 m s^{-1}. At these low velocities and shallow depths it is important to note that there was no noticeable flexing of vegetation, the effect of which can be ignored in such circumstances (Fathi-Maghadam & Kouwen, 1997). In such shallow flows, flow depths varied from point-to-point over the rough bed and around vegetation and so levels were measured using a graduated ruler as point values at the center of the stations (R1–R4). For subsequent analysis, an average of the values recorded at R2 (the upstream fluorometer station) are used, as shown in Table 1 and Figure 5. For each discharge, the flow down the channel was allowed to achieve a steady state such that there was no change in water level during the experiments at each of the four stations (R1–R4; Figure 2a). Wetted channel widths were determined by extrapolating a horizontal surface from the water depth at the point gauges to the banks of the surveyed sections (R1 to R4). In all cases, differences in water depth at the point gauges through time were no more than 0.002 m. At this measurement resolution, the water surface slope, S, found to be typically 4.25×10^{-4}, was calculated from the height of the water surface in the center of each section at R1 through R4 relative to a horizontal datum for each experiment. Water temperature varied between 11 and 12 °C. The tracer used was Rhodamine WT dye, a conservative tracer, which is a preferred environmental water tracer as it does not tend to combine with organic

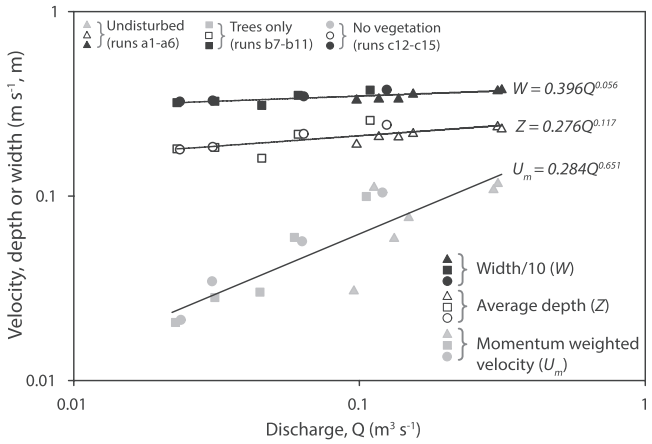

Figure 5. Variation of the momentum weighted velocity (U_m), water surface width (W), and average water depth (Z) at upstream station R2, as a function of the discharge (Q) for all experiments. Values of W have been divided by 10 for convenience of plotting.

matter (Smart & Laidlaw, 1977). Although water tracing can be conducted using concentrations which are invisible to the eye, in the present experiments, visual traces were conducted to observe mixing within the upstream vegetation before dilution occurred downstream, and in addition, higher concentrations should counter any minor loss of tracer due to combination with organic matter. Trials showed that 1 g of dye was a suitable quantity to tag the flows. The dye was injected in the highly turbulent flow immediately below the upstream gate (see Figure 2a) and mixed using a spade across the first 2 m long concrete section to achieve complete visual mixing at a point sufficiently upstream of the first sampling point (R2-17m downstream of the gate). The second dye sampling point (R4) was 37 m downstream of the gate. Once mixed, the dye was uniformly distributed through the depth and width of the flow. As soon as the dye was injected, 50-ml dip samples were taken in the center of the channel every 30 s at both sampling points and sampling continued for a time period which ensured the dye plume had passed through the channel. Up to 90 samples were obtained at each station and returned to the laboratory where the fluorescence of each sample, corrected to a standard temperature, was determined using a calibrated Turner Designs model 10-AU™ fluorometer. The fluorescence values (d_c) were used as direct surrogate measures of dye concentration, as over the range of the observed data the calibration on serially diluted samples was linear, following Turner recommended procedures. On completion of the six experiments (a series), the grass and herbaceous plants were carefully removed throughout the channel and the litter was raked out leaving only the tree stems above a soil bed (Figure 3c). The canopies were removed to facilitate litter removal. Then five experiments (b series) were completed with just the tree stems (Table 1). Subsequently, the trees were carefully cut flush with the soil level and four further experiments (c series) completed (Table 1). In the latter nine experiments, the same procedures were used as for the initial six. Raw fluorescence data are available in Data Set S1 of the supporting information.

2.4. Data Analysis

2.4.1. Dilution Curve Fitting

For each of the 15 experimental tests, data for two concentration curves were collected: the upstream and downstream curve. To utilize the ADZ dilution methodology, the areas (A_c) under the upstream and downstream fluorescence curves should be equal (Figure 4). Using the Matlab Curve Fitting Toolbox™ (Pedregal et al., 2007), spline fits were used to fit curves so as to match areas to better than 5% (see Data Set S1 of supporting information). Trials had shown that for fits to the upstream and corresponding downstream curves poorer than 5%, errors in the determination of final parameter values, such as the Darcy-Weisbach friction factor f, could exceed 15%, but for a range of fits better than 5%, the differences in predicted parameter values were insignificant. For 13 experiments, the single model selected utilized spline fits with 11 breakpoints. The upstream and downstream endpoints of each curve were set to values within 5% of the average measured background values of fluorescence. The quality of the raw data meant that there were no significant outliers in any data series and so no data points were excluded from the analysis. ξ and ζ were calculated using these fitted curves and then checked by comparison with the raw data plots. An example of data and fitted curves is given in Figure 4b. Only for experiments b8 and b9 was it not possible to achieve curve fitting with area differences of less than 5%. For reasons which are unknown, the dilution curves for the downstream section in these two tests were poorly defined, although the upstream curves were well defined. Despite this problem, the first arrival time of the dye at the downstream section was clearly evident in the raw data, while the centroid arrival time was estimated by eye from the raw data curve rather than being calculated using a fitted curve. The results for these latter two experiments were included in the analysis. However, confidence in the values for reach-mean travel times, the ADZ residence times and the dispersive fractions for tests b8 and b9 are less than for the other 13 sets of data. The discharge (Q) for each experiment was determined as follows:

$$Q = \frac{V_t\, m}{\int_0^\infty d_c(t)\, dt} \tag{3}$$

where V_t is the volume of tracer injected and m is the fluorescence value for the injected mass of dye and the denominator is the integrated area (A_c) under either the upstream or downstream time-concentration curve.

2.4.2. Flow Resistance

Values of the reach-scale roughness were determined using the Darcy-Weisbach friction factor f as well as the Manning's n value, where

$$f = \frac{8gRS}{U^2} \tag{4}$$

and

$$n = \frac{R^{2/3} S^{1/2}}{U} \tag{5}$$

The classic flow resistance analysis (e.g., Equations 4 and 7) is based on the law-of-the-wall theory (e.g., Buschmann & Gad-el-Hak, 2003). There, R is the hydraulic radius (= A/P) where A is the cross-sectional area from topographic survey and P is the wetted perimeter of the channel cross section. Values of A and P were obtained from the geometry of the cross section R2 (e.g., Figure 2b) using the average water depth at this station for each run, and g is the acceleration due to gravity. The Manning formula strictly applies for fully rough-turbulent flow, that is, under flow conditions for which the flow resistance is independent of Reynolds number and herein some of the experimental conditions represent transitional-turbulent flow. However, as Manning number is used extensively, we take the opportunity (see section 4.1) to demonstrate that recommended values of n in standard texts may not be appropriate for vegetated channels. The longitudinal mean velocity U (see Equations 4 and 5) for the reach may be calculated in three ways: As the first arrival velocity; $U_{1st} = L/(\xi_d - \xi_u)$ where L is the distance between R2 and R4; as the momentum-weighted velocity; $U_m = L/\zeta$; and as the area-weighted velocity; $U_A = Q/A$. The use of U_{1st} or U_m in deriving roughness values is discussed by Richardson and Carling (2006).

The total friction factor f is traditionally partitioned between the grain resistance f' and form resistance f'' (Afzalimehr et al., 2010; Yalin, 1977) where the latter is generated by energy losses associated with irregularities in the shape of the channel. Here a somewhat different approach is taken as the friction includes both the vegetative flow resistance f''' as well as the resistance of the channel boundary. Thus, the total friction can be characterized as follows:

$$f = f' + f'' + f'''. \tag{6}$$

In addition, the expected value of the grain roughness of the earthen bed [without form roughness] can be estimated as (van Rijn, 1984) follows:

$$\sqrt{\frac{1}{f'}} = 2.03 \log\left({}^{12.2Z}/_{d_r}\right) \tag{7}$$

where d_r is the characteristic roughness length of the bed. All derived metrics can be found in Data Set S1 of the supporting information.

3. Results

3.1. Hydraulic Geometry of the Channel

In all the experiments, the flow remained in-channel, that is, flow depths (Table 1) were less than the bank-full condition of $Z = 0.5$ m. As a test of the quality of the data, the at-a-station hydraulic geometry is calculated for the upstream station R2 (Figure 5); the data scatter is small, the constants of the power functions approximately multiply to unity and the exponents approximately sum to unity as expected

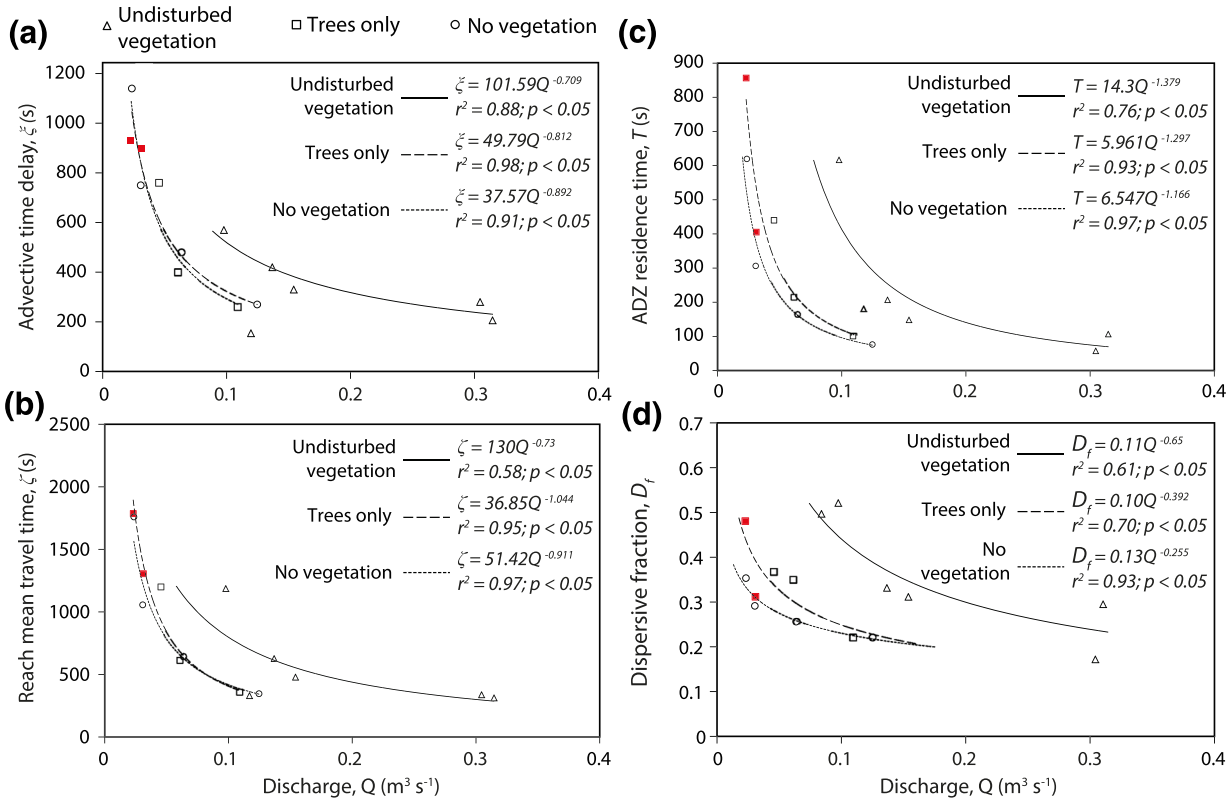

Figure 6. Variation in (a) the advective time delay, (b) the reach mean travel time, (c) the ADZ residence time, and (d) the dispersive fraction as functions of discharge and vegetative cover. Red symbols denote runs b8 and b9, where curve areas were not fit to within the 5% tolerance as per all other runs (see discussion in section 2.4.1). Note that these data points are still included in the fitted power regression.

(Ferguson, 1986; Leopold & Maddock, 1953). A simple power function describes the data trend for discharge with depth which can be written as follows:

$$Q = j_5 Z'^{j6} \tag{8}$$

using the notation of Richardson and Carling (2006), where $Z' = Z + Z_o$. The adjustment to Z maximizes the R^2 value of the regression curve when the datum value Z_o is 0.01 m where the parameters j_5 and j_6 are determined from least squares regression. Equation 8 is utilized in section 3.3 to determine the celerity of the flood wave without storage. The Reynolds number ($R_e = U_m Z/\nu$), where ν is the kinematic viscosity (here about $1.2{\cdot}10^{-6}$ m^2/s for 11.5 °C), varied between 2,000 and 22,000 with Froude numbers ($U_m/\sqrt{gZ}$), between 0.01 and 0.05. The primary response of flow to vegetation removal was a small increase in bulk velocity, with depth and wetted width decreasing only slightly.

3.2. ADZ Parameters From Concentration Data

The ADZ analysis determines the advective time delay (ξ), the reach mean travel time (ζ), the residence time (T) of the tracer, and the dispersive fraction (D_f) with changes in discharge and vegetation cover (Figure 6). Prior investigations (see references in Richardson & Carling, 2006) have found that either an inverse law or a power law fit the ADZ parameter trends well. In this instance, there are too few data available for each treatment to be definitive, but considering the trend of all the data in Figure 6, a power function provides a higher R^2 value than an inverse function and so least squares power functions are fitted to each treatment. It is evident that both the advective time delays and the reach mean travel times reduce as both discharges increase and also as vegetation is successively removed. Of particular note is the fact that the presence of undisturbed vegetation has the biggest influence in increasing the values of all four parameters represented in Figure 6. For any chosen reference discharge, the presence of trees alone on an earthen bed only has a

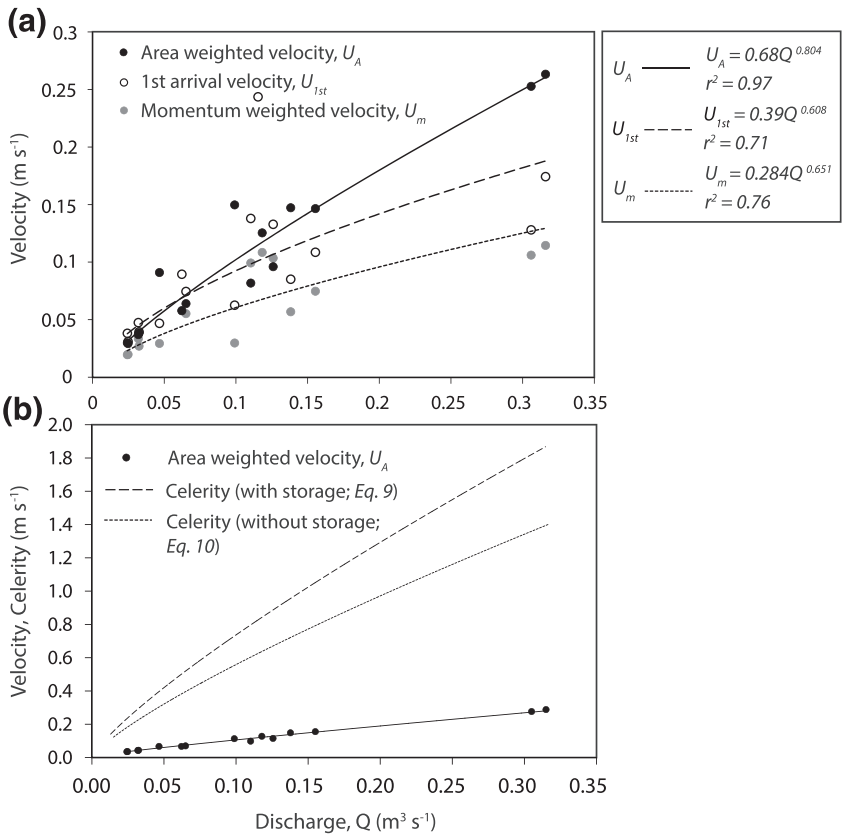

Figure 7. (a) Characteristic variation in reach velocity measurements as a function of discharge. (b) Calculated celerity and measured area-weighted velocity as a function of discharge. Celerity has been determined using two methods (see text for explanation).

marginally greater influence, in contrast to parameter values associated with an earthen channel. However, importantly, in all experiments, the parameters trend toward a constant low value for high discharges as has been noted more widely (Beven & Carling, 1992; Green et al., 1994; Wallis et al., 1989, 1990) among others.

It is evident that there is a decline in the dispersive fraction as discharge increases and as vegetation is successively removed, such that at high discharges the dispersive fraction approaches a value of around 0.2. It is unfortunate that there are few data for high discharges. Nonetheless the trend is clear; the dispersive fraction can be comparable for both undisturbed vegetation and rough bare earth channels at high discharges but not for low discharges. This interpretation is supported by the overall reduction in the dispersion time scales seen in Figure 6 and as discharge increases. Taken together, these results indicate that retentiveness due to the presence of sparse vegetation becomes increasingly insignificant at relatively high discharges. This result is consistent with the initial hypothesis that flow retardation is greater for low discharge, low Reynolds number flows, and retardation declines as vegetation is removed but that at higher discharges with higher Reynolds numbers retentiveness of vegetated floodplains is not dissimilar to a bare earth surface.

3.3. Velocity and Celerity

As noted in section 2.4.2, the reach mean velocity was calculated in three ways: as the first arrival velocity, as the momentum-weighted velocity, and as the area-weighted velocity. In agreement with theory, the first arrival velocity for a pulse injection is greater than the momentum-weighted velocity and the area-weighted velocity (Figure 7). It may be observed that U_m increases almost monotonically as a power function of discharge. As expected, U_A has broadly similar, although lower, values to U_m at low discharges but diverges slightly as discharge increases. Whereas some difference is always to be expected in these two estimates of velocity, the systematic difference in the trends of U_A and U_m can be interpreted in only two ways. Either the discharge estimate from Equation 3 is too large, or no specific part of the channel is

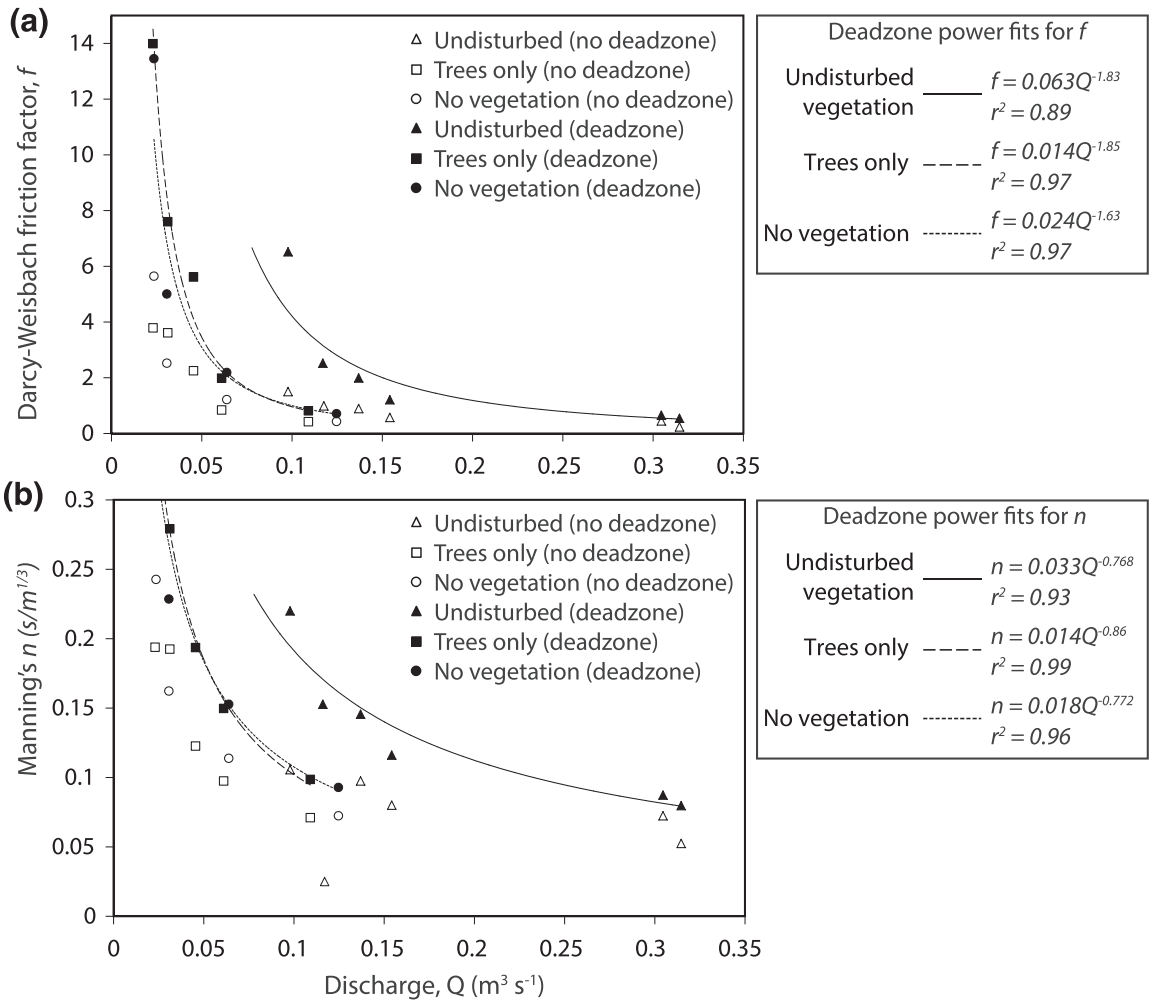

Figure 8. (a) Variation of the Darcy-Weisbach friction factor as a function of discharge and vegetation cover. For clarity, the power function general trends are fitted to the "with dead zone data only." (b) Generalized power function trends for variation in Manning's n as discharge and vegetation cover vary.

acting only as storage but rather the majority of the volume of the channel is subject to fluid retention effects. Given that the values of A_c used in Equation 3 agree to within 5% suggests the error, if any, in the discharge estimate might be due to inaccurate estimation of the value of the fluorescence value of the mass of dye injected. However, there is no basis to question the fluorescence calibration; thus, the slightly divergent trend must reflect the fact that fluid retention within the whole channel is important rather than any specific areas within the channel playing a disproportionate effect as discharge changes. If the latter effect was important, for any given range of discharge values, then U_A would diverge *downward* below the U_m trend (Richardson & Carling, 2006; their Figure 8a).

The interpretation of the velocities noted above is reinforced by consideration of the kinematic wave speed, that is, the celerity (c) of the flood wave: (1) without storage and (2) with storage. The first method considers the rate of change of discharge with cross-sectional area (Beven, 1979) and is detailed in Richardson and Carling (2006; their Equations 24 and 25). Richardson and Carling (2006) assumed a trapezoidal cross section and a Gompertz equation fit to Q data as a function of Z. Consequently, the following expression for celerity with storage is derived:

$$c = j_5 j_6 (Z + Z_o)^{j_6 - 1} \frac{\tan \propto}{2Z + \beta \tan \propto} \tag{9}$$

where j_5, j_6 are constants, α is the characteristic slope of the channel sidewalls, and β is a constant equal to the breadth of the floor of the channel which is also assumed to be trapezoidal (compare Figure 2b).

Equation 9 is plotted in Figure 7b with $Z_o = 0.01$ m, $\alpha = 15^0$ and $\beta = 4$ m. Celerity can also be determined by differentiating the study-reach volume-discharge relationship (Richardson & Carling, 2006; their Equations 26 to 28). Using the latter approach then celerity without storage is given by

$$c = k_7 Q^{k_8} \tag{10.1}$$

where

$$k_7 = \frac{L}{k_5 k_6} \tag{10.2}$$

and

$$k_8 = 1 - k_6 \tag{10.3}$$

where k_5 and k_6 are the fitting parameters in the reach volume–discharge power law relationship:

$$V_r = k_5 Q^{k_6}. \tag{10.4}$$

In Figure 7b, it may be seen that the estimates of celerity using the two methods are similar at low discharges but diverge at higher discharges. Both methods consider celerity as a function of changing discharge with cross-sectional area, but the first method utilizes tracer dilution data (to obtain Q) and topographic survey (to obtain A) while the second method utilizes only tracer dilution data (to obtain Q and A). Thus, the divergence of the area-weighted velocity from the momentum-weighted velocity (Figure 7a) is due to a change in the volume of the reach utilized as storage. In this case, the first method represents celerity with storage whereas the second method represents the celerity as if the main flow was within a smaller channel section that excludes any marginal storage. The curve for celerity with storage does not fall below the trend of the reach mean flow velocity (Figure 7b). Thus, from a consideration of conservation of mass, no significant areas of the channel act only as storage and do not contribute to discharge. Rather the ADZ area (as conceptualized in Figure 4a) is a discharge dependent quantity, related to delayed flow, rather than a region or an aggregate of regions of static fluid. This final observation is important as it indicates that *transverse mixing across the breadth of the reach is highly important for all discharges* and for *all vegetative treatments* and is due to reach-scale roughness induced collectively by the ground cover, the tree trunks and the channel boundary.

In section 3.4, the ADZ derived data are used in a novel manner to "decouple" and evaluate the roughness of the (a series) undisturbed vegetation, the (b series) trees with bare earth, and the (c series) bare earth, as both the discharge and the Reynolds number of the flows vary.

3.4. Channel Roughness

Two estimates of the reach mean velocity (U_{1st} and U_m) were used in Equations 4 and 5 based on the advective time delay and the mean travel time to obtain two estimates of flow resistance for the range of experiments (Figure 8a). Because Equations 4 and 5 are related, a similar analysis for Manning's n produces similar results which, for clarity of presentation, are illustrated in Figure 8b. In both parts of the figure, data and fitted power curves are shown for the case of reach mean travel time (i.e., with dead zone effect) but only the data are shown for the case of advective time delay (no dead zone effect). Manning's n tends to fall to a constant value of approximately 0.05 for higher values of discharge, which is consistent with many prior field investigations of vegetated channels (Wu et al., 1999).

The travel time of water that is not impeded by dead zone mixing is represented by the advective time delay (Figure 8a) and that time is equivalent to an aggregated dead zone of zero volume, producing corresponding values of ($f' + f''$). These values exclude dead zone effects that in a straight, heavily vegetated, channel are due mainly to the presence of the vegetation. In contrast, calculation using the reach mean travel time (Figure 8a) produces values of ($f' + f'' + f'''$). For all vegetation types, the roughness ratio ($f' + f'' + f'''$)/($f' + f''$) decreases from a value of 4 for near-zero discharge trending asymptotically toward approximately 1.5 for high discharges.

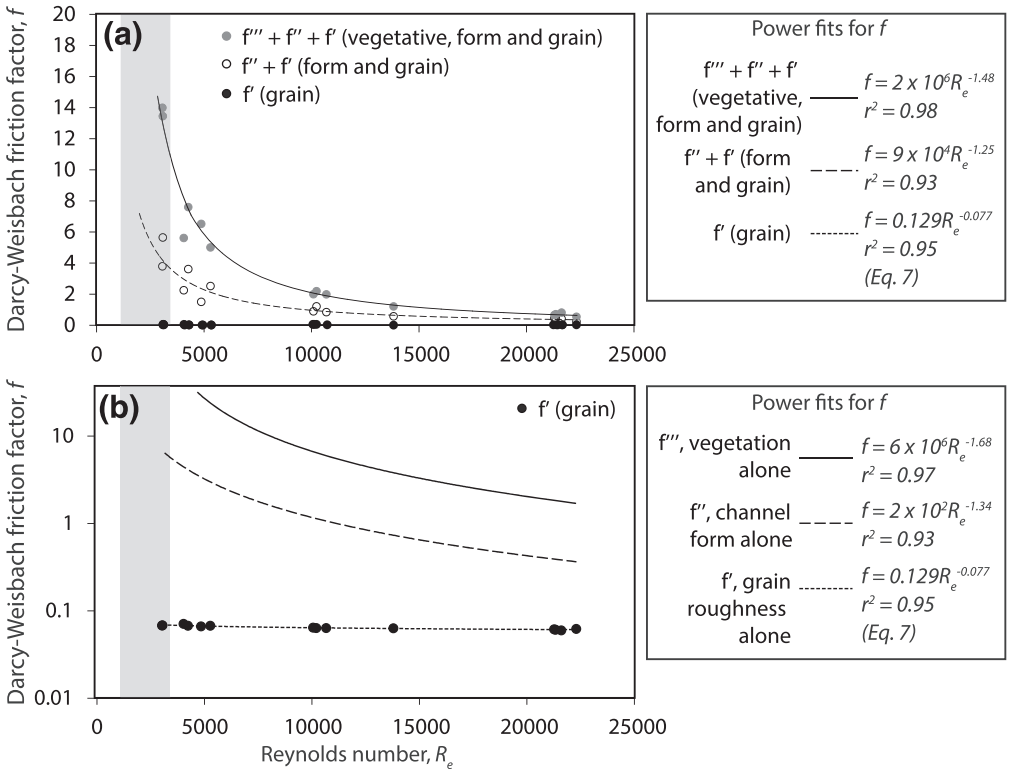

Figure 9. (a) Variation in the flow resistance f components as function of the Reynolds number. (b) Variation in the isolated flow resistance f components as a function of the Reynolds number (see text for an explanation). A log scale for f is used in panel (b) to show the trend of the grain roughness clearly.

Although the proportioning of flow resistance in the manner outlined above (i.e., vegetation, channel form, and grain roughness) is not strictly exclusive, it is evident that by subtracting the trend of the curve representing advective time delay from the mean travel time will provide values for vegetative resistance alone, provided the grain resistance can be estimated.

Rather than represent flow resistance as a scale-dependent function of discharge, Figure 9 represents the dependency of f on the scale-independent Reynolds number. The pale-gray shaded area represents the range of *Re* values normally associated with transitional turbulence within stem-filled flows (Soulitis & Prinos, 2008), with values to the right representing fully turbulent conditions. Values of f for sand channels are usually in the range 0.01 to 0.1 (Raudkivi, 1967; Yalin, 1977); however, in the current study, $f' + f'' + f'''$ never falls below unity and $f' + f''$ falls below unity only for R_e greater than about 12,000. The roughness length for the heterogeneous rough earth bed cannot be known with any certainty, but the results of solving Equation 7 for measured values of depth are presented in Figure 9 assuming a relatively coarse value of d_r of 3 cm; the predicted data values range between $f' = 0.069$ and 0.059, decreasing as the Reynolds number increases. The difference in the trend of Equation 7 and the observed values of f for vegetated conditions and the bare earth channel is striking whatever reasonable value of d_r is selected.

The long-dashed line in Figure 9b is produced by subtracting the trend for $(f' + f'')$ from $(f' + f'' + f''')$ in Figure 9a, and the solid line is produced by subtracting f' from $(f' + f'')$. In this manner, contributions of the channel roughness and the vegetative roughness are quantified and isolated.

4. Discussion

In the following discussion, the reasons why there is variability in the contributions to friction and mixing of herbaceous vegetation, trees, and the earthen boundary of the channel is first explored. Latterly, a more general consideration is given to mixing processes in floodplain flows not least because the results from the present series of experiments utilize a novel procedure. In that respect, a comparison is made between the

present approach and a previously published methodology, which seeks to discriminate significant factors contributing to lateral mixing in flows wherein longitudinal mixing dominates, as here.

4.1. Contributions to Friction in Vegetated Floodplains

In the relevant parameter plots, the data scatter tends to be more pronounced in the case of the mixed community of grass, herbaceous plants, and trees. In principle, data scatter could reflect incomplete initial mixing in the experiments but there is no basis for suspecting this as a factor in the first six experiments conducted using a mixed vegetation cover. Rather, this result is comparable with the findings of Hui et al. (2010) and Järvelä (2002) who noted increased scatter in values of the *en masse* drag coefficient and friction factor for mixed grass-shrub communities in contrast to isolated arrays of shrubs.

The ADZ residence times (Figures 6a–6c) and the dispersive fractions (Figure 6d) clearly discriminate between the undisturbed vegetation and the bare earth conditions, with a distinct reduction in fluid retention as vegetation is removed. The effect of retaining a tree cover (with no understory), in contrast to a bare earth channel, has a less pronounced effect on parameter values than retaining all the vegetative cover. It was noted in section 3.2 that the role of vegetation in fluid retention rapidly decreases in significance at higher discharges, thus supporting the initial hypothesis. It appears (Figures 7 and 8) that the effect of vegetation on dispersive processes is evenly distributed across the complete section and throughout the reach as discharge and turbulence varies. This behavior seems typical of turbulent flow through emergent vegetation (Stoesser et al., 2010), although there are exceptions (Naot et al., 1996a), and can be contrasted to the importance of distinctive and localized marginal storage zones developing in unvegetated river systems (Jackson et al., 2013; Richardson & Carling, 2006).

The ADZ framework proved useful to extract components of the Darcy-Weisbach values of the hydraulic roughness f as well as values of Manning's n. The range of values of f or n for undisturbed vegetation are distinct from the trees-only and the bare earth conditions. Despite the clear discrimination afforded by the dispersive fraction data, the f data do not distinguish the behavior of the trees only from the bare earth conditions when considered as a function of discharge and Reynolds number (Figures 8 and 9, respectively). In part, this is due to the fact that well-spaced tree-like rods have flow resistance characteristics not dissimilar to a bare channel (Naot et al., 1996b; Perucca et al., 2009), and vegetative resistance tends to decline at higher Reynolds numbers toward the bare earth values. However, considered as a function of the Reynolds number the separate components of flow resistance due to the earth, the channel form and the vegetation are discriminated (Figure 9). Often laboratory studies have considered the bed roughness to be insignificant compared with the vegetative roughness (Hoffman, 2004; Nepf, 1999b; Wu et al., 1999), and in the present case, the grain roughness is minor compared with the form and vegetative roughness (Figure 9). However, as noted by Righetti (2008) and Tanino and Nepf (2008) for natural and seminatural flows, the channel-form resistance can remain a significant contribution to the total friction (Figure 9).

The gradient of the f:R_e functions decline as vegetation is removed (a result also observed by Järvelä, 2002) with high friction factors notably associated with low Reynolds numbers and the presence of a herbaceous understory. The range of exponents in the f:R_e functions depicted in Figures 8a and 9 is very similar to those reported previously for partially submerged vegetation (Wu et al., 1999; their Figure 6). However, the variation in the roughness comparing vegetative states cannot just be explained by progressive inundation of the understory by higher water levels. Average water depth at R2 is only a very weak positive function of discharge (Figure 5 and Equation 8) with water depths here ranging between 0.16 and 0.26 m for all experiments. Although f declined sharply as depth increased, the effects of the differing vegetative treatments on f could not be isolated as a function of depth, which suggests that turbulent intensity rather than relative inundation of vegetation controls the friction values.

In some respects, the results from the present series of experiments cannot be compared directly with most prior published experimental data on flow resistance as most of the latter have used isolated woody elements in hydraulic flumes, but there are some commonalities. In particular, the flow resistance is significant for transitional flow conditions and reduces for increasing values of Reynolds number for fully turbulent flow (Figure 9). In most laboratory experiments, the hydraulic roughness due to vegetation is estimated based on relationships, which scale up from consideration of the drag on isolated elements to groups of elements (Naot et al., 1996b). For example, Hui et al. (2010) use a variant of the Linder (1982) relationship:

Table 2
Typical Manning's n Roughness Factors for Engineered Channels as Cited by LMNO Engineering, Research, and Software, Ltd. Web Site Accessed in 2016

	Manning's n[a]	Darcy-Weisbach f[b]
Excavated Earth Channel[a]		
Clean Earth	0.022	0.066
Gravelly	0.025	0.09
Weedy	0.03	0.12
Stony	0.035	0.17
Light Brush	0.05	0.35
Heavy Brush	0.075	0.75
Trees	0.15	3

[a]Source: http://www.lmnoeng.com/literature.htm. [b]Approximate equivalent f values to column 2 values of n: $n = \sqrt{f\left[\sqrt{Z^{1/3}/8g}\right]}$.

$$f = \frac{4C_d A_p}{a_x a_y - V_{veg}\frac{1}{Z}} \tag{11}$$

to demonstrate the positive correlation of the *en masse* drag coefficient C_d with an estimate of the total friction in vegetated arrays, where A_p is the frontal area of the vegetation, a_x and a_y are the downstream and transverse spacing of the vegetative element trees, and V_{veg} is the volume of the vegetation. Several studies (reviewed by Järvelä, 2004) conclude that C_d for arrays of isolated small trees is around 1.5 which would accord with Naot et al. (1996b) and Fathi-Maghadam and Kouwen (1997) who concluded that friction in emergent well-spaced trees is independent of Reynolds number for high velocities. Yet for mixed communities of flume-planted shrubs and trees, similar to the present experiments, Hui et al. (2010) report C_d values of 10 to 30 for transitional *Re* values and dense planting, increasing rapidly as Reynolds number reduces. These values equate to f values of up to five, which result is commensurate with the range of f''' values noted in Figure 9 for transitional to fully turbulent conditions.

Thus, the natural vegetation cover studied in the present experiments tends to produce roughness values that are much larger than expected from frequently used resistance relations, artificial arrays of elements (see also Ishikawa et al., 2000; Järvelä, 2002; Shucksmith et al., 2011), and slightly higher than the mixed planting conditions of Hui et al. (2010). In part, this may be due to the trees being clumped, which configuration tends to produce higher drag than aligned trees (Ming & Shen, 1973; Righetti & Armanini, 2002). In particular, the results, including the limited range of exponents of the relationships between f and *Re* for vegetative conditions, are comparable with the results of Lee et al. (2004) for *f*:*Re* field and flume data for emergent coarse grasses above a dense litter layer.

In part, these discrepancies and similarities, respectively, may be explained by the fact that some experimental studies may underestimate roughness often as they determine the flow blocking by vegetation as due to frontal area (A_p) alone (Equation 11), neglecting vegetation volume (V_{veg}), whereas the ADZ model accounts for this volumetric effect of vegetation. In particular, the roughness expressed as Manning's n is significantly higher for low discharges and low Reynolds numbers than is commonly assumed in the engineering literature (see Table 2) but falls to comparable values for high discharges and high Reynolds numbers. For example, for a reference discharge of 0.1 $m^3 s^{-1}$, Manning's n reaches nearly 0.2 s $m^{1/3}$ in the present experiments for tree and herbaceous cover but falls to less than 0.10 s $m^{1/3}$ for bare earth conditions. The former value is similar to n values reported for mangrove root masses of similar stem densities and water depths (Mazda et al., 1997; Wolanski et al., 1980) as for the present experiments but can be contrasted to the typical engineering recommendations shown in Table 2 and reported elsewhere (Arcement & Schneider, 1989; Barnes, 1967; Cowan, 1956), which would be too low if applied to the present experimental channel for all situations bar the highest discharges.

4.2. Mixing in Floodplain Flows

For all flow conditions investigated, vegetative resistance to flow is relatively high especially when turbulence (as indexed by the Reynolds numbers) is low, including for transitional flow conditions. In situations where the flow depth is substantially greater than the height of the herbaceous vegetation, the trend to a constant low value of resistance may be accredited to the slight resistance of flow through the vegetation in contrast to the unimpeded flow above (Chow, 1959; Temple et al., 1987; Wu et al., 1999). However, when, as in the present experiments, the herbaceous vegetation is not deeply inundated, the trend to a constant low resistance value reflects the importance of mechanical mixing across and throughout the reach even at low velocities (Helmio, 2004; Naot et al., 1996b; Perucca et al., 2009) in contrast to the role of turbulence and molecular diffusion. This important observation links back to the concept outlined in the introduction that the balance between longitudinal mixing (K_t) and transverse mixing (K_m) is moderated by the presence of vegetation and so this is now considered further. Because the application of the ADZ methodology to

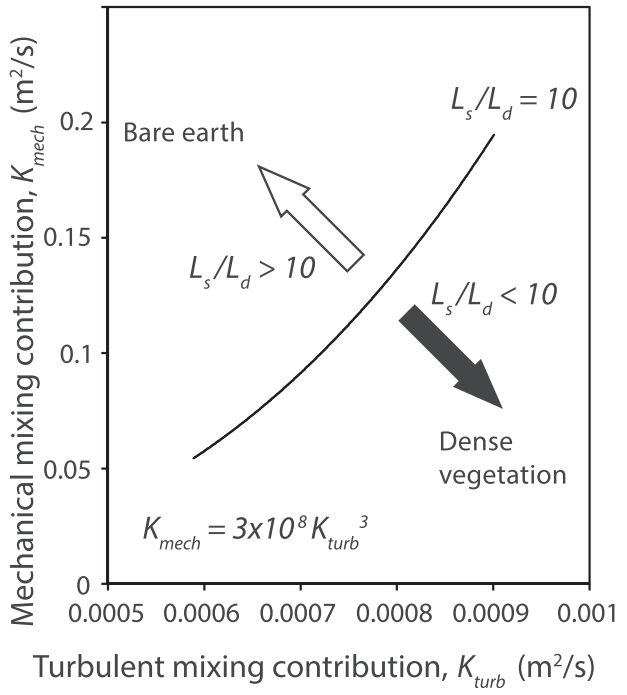

Figure 10. Relationship between the contributions of turbulent mixing and mechanical mixing to total lateral mixing. The power fit and open circles represent the data for the "trees-only" runs (b7–b11) according to Equations 13 and 14. Increasing values of both parameters are largely conditioned by the velocity, U_{1st}, mediated by vegetation spacing (L_s), and bole diameter (L_d). For these runs, the ratio of L_d to L_s was 10, represented by the fitted regression. The black arrow indicates the general direction in which the curve would shift, for a constant value of U_{1st}, as the vegetation density is increased (i.e., L_s decreased). The white arrow indicates the reverse, a decreasing density of vegetation.

vegetative flows is novel, below the general consistency of the results with another approach (Nepf, 1999b) is demonstrated.

The total flow mixing term (K_{total}) may be considered to be

$$K_{total} = K_t + K_m + K_d$$

where K_d is the effective molecular diffusion coefficient of the fluid (Grathwohl, 1998). The latter parameter will vary with vegetation density but is a very small contribution to K_{total} and is neglected herein. Thus, the ratio of K_t/K_m is of particular interest. In the absence of vegetation, which induces lateral flow around stems and wake production, the turbulence component of mixing is greatly reduced and mixing is dominated by mechanical mixing, chiefly in the longitudinal direction but mechanical mixing also contributes to lateral dispersion (Nepf, 1999b). Thus, although the turbulence component makes a substantial contribution to K_m when vegetation is dense, the mechanical contribution is likely more important to transverse mixing in the case where vegetation is absent and K_t is dominant.

This final observation is made clear by plotting the turbulent mixing contribution (K_{turb}) in relation to the mechanical mixing contribution (K_{mech}) (Serra et al., 2004), which are parameters analogous to K_m and K_t, respectively. It is assumed that transverse mixing is due both to turbulent dispersion of fluid packages and to mechanical transverse fluid displacement due to the quantified presence of plant stems as well as the development of multiple mini "dead zones" in the wakes of stems (Nepf et al., 1997):

$$K_{turb} = \gamma(UL_d)\left[\left(\frac{L_d}{L_s}\right)^2 (C_d)\right]^{1/3} \quad (13)$$

$$K_{mech} = (UL_d)\left(\frac{\gamma_1^2}{2}\right)\left(\frac{L_s}{L_d}\right)^2 \quad (14)$$

The coefficients γ and γ_1 are both set to 0.9 (Nepf, 1999b) for similar stem-density experiments, and L_s and L_d are length scales related to the spacing of trees and the stem diameters. These are scaling factors that appear in both equations, and here they are set to $L_s = 0.5$ m and $L_d = 0.05$ m for the current tree experiments (as these are the values that would apply if all the trees were evenly spaced). Equations 13 and 14 (Serra et al., 2004) are due to physics-based considerations (Nepf, 1999b) with $C_d = 2gZA_fS/\eta_p A_p U^2$ (Wu et al., 1999) (A_f is the frontal area of flow and η_p is a vegetation porosity) and mixing expressed effectively as an average of a spatially varying flow field, but there are few data sets for low Reynolds numbers to ascertain the validity of this approach (Serra et al., 2004; Västilä et al., 2016). Nevertheless, the equations are applied to the current tree data to demonstrate the approximate scaling relationship between K_t and K_m in the current test conditions (Figure 10). It is evident that transverse mechanical mixing in such low Reynolds number flows, as indexed by K_{mech} is typically three orders of magnitude greater than the transverse turbulent dispersion contribution, as indexed by K_{turb} (as noted in Figure 10). The two parameters are related by a power function such that mechanical mixing (due primarily to increased flow velocity) becomes more important in more turbulent flows but the turbulent component continues to increase in the faster flows (Re $\rightarrow 10^4$; Nepf et al., 1997).

Note that Equations 13 and 14 pertain to well-defined plant stems with regular spacings. Consequently, it is not possible to apply the analysis to the undisturbed vegetation or the bare earth examples. In the first case, there are no L_s and L_d data and in the latter case there is no vegetation, although bed roughness will still

instigate mechanical and turbulent mixing. Nevertheless, it is evident that the more complex canopy in the case of undisturbed vegetation will have greater stem densities and smaller plant stems as herbs as well as trees are represented. Assuming the coefficients γ and γ_1 both equal 0.9, for higher density vegetation, and reducing the stem spacing for the given stem diameter to simulate denser vegetation, it is evident in Equations 13 and 14 that the undisturbed vegetative examples would plot to the right of the curve for the trees only. Similarly increasing stem spacing for the given stem diameter, to represent sparse trees on bare earth, data would plot to the left of the curve. However, if the stem diameter also is modified, reduced, for example, then overlapping data points can occur for different vegetation covers. Data sets for different vegetative treatments thus can overlap, as high dispersion can occur during high discharges for given vegetative situations as well as for bare earth conditions. Thus, for different discharges, there is no absolute range of dispersive conditions and, by analogy roughness conditions, associated uniquely to a given vegetative state. Thus, this result is consistent with the possibility of having the same dispersive fraction recorded for different vegetative states (Figure 6d) as discharge is varied.

Although these experiments were made in a confined channel, the flows were broad and shallow not dissimilar to shallowly inundated floodplain hollows on scrub-covered floodplains. Mixing parameter values on the largely flat, low-amplitude vegetated surfaces between hollows might be slightly different to those reported herein. Nonetheless, the general behavior of flow over these more elevated surfaces should be similar to the behavior within the hollows, as Reynolds numbers and discharges vary. However, caution should be exercised in extending these results to flow substantially deeper than those reported here (> 0.3m). In particular, the results are unlikely to pertain to the complex flow that occurs along the bank line of a river. This riparian location is subject to significant transverse shear, enhanced turbulent mixing, and complex secondary currents (Babaeyan-Koopaei et al., 2002; Carling et al., 2002).

Taken together these results are significant for modeling flow across forested floodplains especially in relation to the significance of zones of vegetated, slow, shallow flow away from the riparian zone. In the higher speed, higher Reynolds number zones ($10^3 < Re < 10^4$ or higher), the roughness coefficient in the sparse vegetation is not dissimilar to that within an earthen channel. However the slow-flow zones (stands of dense vegetation) may be spatially dispersed across a floodplain adjacent to zones of locally faster flow between the stands (Harwood & Brown, 1993; Jeffries et al., 2003; Piégay et al., 1998), or they may be riparian; adjacent to open channels wherein the flow rates and mixing rates are higher (Kobashi & Mazda, 2005). However, slow-flow areas may concentrate pollutants and nutrients especially as these slow areas trap more sediment than faster flowing areas (Jeffries et al., 2003; Nicholas & Walling, 1998). Thus, when modeling flows in the riparian zone, the strong gradient in roughness and dispersion across the riparian region would not be effectively reproduced using traditional values of roughness, such as Manning's n (Table 2) to calibrate the flow models. Further, the flow pathways between plant stems are likely to be complex with mechanical mixing promoting fairly homogeneous deposition between stems and stand patchiness promoting the development of shear zones (Naot et al., 1996a) and preferential flow and depositional pathways.

5. Conclusions

Dispersion of a dye tracer is a simple but powerful tool to derive bulk hydraulic data for vegetated channels. The ADZ model in particular produces parameters that reflect the fluid retention properties of the flow due to the presence of vegetation. These parameters can be interpreted generally as the effect of aggregated "dead zone" storage in the reach, but in the case of well-spaced vegetation, the storage terms are better considered as indicative of the degree of lateral and longitudinal mixing across the section and throughout the reach volume rather than viewed as a single (or a series) of discrete fluid retention zones.

For the forested floodplain analogue that was the focus of this study and for very shallow flows, the primary response of flow to vegetation removal was a small increase in bulk velocity, with depth and wetted width decreasing only slightly. Nonetheless, it is shown that the effect of vegetation on the Darcy-Weisbach flow resistance factor decreases as a function of the Reynolds number. Each vegetative cover displays a distinct individual trend, but these tend to approach a minimum value for high discharges. The key point here is that sparse vegetation has a significant effect on forested floodplain fluid retention at low flows but at the high flows become negligible.

In the same vein, the common engineering roughness factor, Manning's n, also approaches a minimum value for fully turbulent flow as discharge increases in accord with recommendation in the engineering literature but assumes substantially high values for transitional turbulence conditions. The increasing dominance of section-wide and reach-length mixing in a channel at higher discharges means that different vegetative covers can exhibit the same mixing parameter values as a bare earth channel depending on the reference discharge value selected. The key point here is that as discharge increases on forested floodplains, fluid retention declines toward the same value regardless of vegetation composition. This latter effect is demonstrable using values of the turbulent mixing contribution and the mechanical mixing contribution to transverse dispersion, revealing an increased contribution of mechanical mixing in higher density vegetated flows that reduces as vegetation is removed. The key point here is that as vegetation density increases, lateral mixing becomes increasingly more dominant (relative to longitudinal) than for less dense cases.

Taken together, these results indicate that when managing vegetation type and density in relation to selecting flow resistance parameter values, careful consideration must be given to the flow Reynolds numbers anticipated and the density of the tree cover; otherwise, no effective changes in bulk flow behavior will necessarily be achieved.

List of Notation

A	Effective cross-sectional area
A_c	Area under the time-concentration curve
A_f	Frontal area of flow within and above vegetation
A_p	Frontal area of vegetation
A_x	Downstream spacing of vegetation elements
A_y	Transverse spacing of vegetation elements
c	Celerity
C_d	Drag coefficient
D_f	Dispersive fraction
d_c	Fluorescence values
d_r	Bed sediment roughness length
f	Darcy-Weisbach friction factor
f'	Darcy-Weisbach grain resistance factor
f''	Darcy-Weisbach channel form resistance factor
f'''	Darcy-Weisbach vegetative resistance factor
g	Acceleration due to gravity
j_5, j_6	Constants in the flood wave celerity calculation
k_5, k_6, k_7, k_8	Parameters in the flood wave celerity (without storage) calculation
K_d	Effective diffusion coefficient
K_m	Transverse mixing coefficient
K_{mech}	Mechanical mixing coefficient
K_t	Longitudinal mixing coefficient
K_{total}	Total flow mixing term
K_{turb}	Turbulent mixing coefficient
L	Distance between sampling stations
L_d	Bole diameter
L_s	Tree spacing
m	Fluorescence value of initial dye tracer
n	Manning's n (coefficient of roughness)
P	Wetted perimeter
Q	Discharge
R	Hydraulic roughness
R_e	Reynolds number
S	Water surface slope
T	ADZ residence time or mixing time
U	Longitudinal mean velocity

U_{1st}	First arrival velocity
U_A	Area weighted velocity
U_m	Momentum weighted velocity
V	Aggregated dead zone volume
V_r	Study reach volume
V_t	Volume of dye tracer
V_{veg}	Volume of vegetation
W	Water surface width
Z	Water depth
Z_o	Reference depth
α	Slope of channel side walls
β	Breadth of channel base
γ, γ_1	Constants in the turbulence and mechanical mixing calculation
η_p	Vegetation porosity
ν	Kinematic viscosity
ξ	Advective time delay, $\xi_d - \xi_u$
ξ_u, ξ_d	First arrival time of the concentration curve at the reach entry (upstream) and exit (downstream) sampling locations
ζ	Reach mean travel time, $\zeta_d - \zeta_u$
ζ_u, ζ_d	Centroid of time-concentration curves at the reach entry (upstream) and exit (downstream) sampling locations

Acknowledgments
We acknowledge use of the University of Southampton Chilworth Hydraulic Facility. Karl Scammell and James White provided technical support at the flume and Peter Morgan calibrated the fluorometer and assisted in processing the samples. The comprehensive and insightful comments of the Associate Editor, Ian Rutherfurd, and the three anonymous referees on the initial submissions were invaluable in preparing the final version of this manuscript.

References

Aberle, J., & Järvelä, J. (2013). Flow resistance of emergent rigid and flexible floodplain vegetation. *Journal of Hydraulic Research, ASCE*, *51*(1), 33–45. https://doi.org/10.1080/00221686.2012.754795

Afzalimehr, H., Singh, V. P., & Najafabadi, E. F. (2010). Determination of form friction factor. *Journal of Hydrologic Engineering*, *15*(3), 237–243. https://doi.org/10.1061/(ASCE)HE.1943-5584.0000175

Arcement, G. J., & Schneider, V. R. (1989). *Guide for selecting Manning's roughness coefficients for natural channels and flood plains, United States Geological Survey Water Supply Paper 2339*.

Babaeyan-Koopaei, K., Ervine, D. A., Carling, P. A., & Cao, Z. (2002). Velocity and turbulence measurements for two overbank flow events in River Severn. *Journal of Hydraulic Engineering, ASCE*, *128*(10), 891–900. https://doi.org/10.1061/(ASCE)0733-9429(2002)128:10(891)

Barnes, H. H. (1967). *Roughness characteristics of natural channels*, *United States Geological Survey Water Supply Paper 1849* (pp. 1–213). Washington: US Government Printing Office.

Beer, T., & Young, P. C. (1983). Longitudinal dispersion in natural streams. *Journal of Environmental Engineering, ASCE*, *109*(5), 1049–1067. https://doi.org/10.1061/(ASCE)0733-9372(1983)109:5(1049)

Bennett, S. J., Pirim, T., & Barkdoll, B. D. (2002). Using simulated emergent vegetation to alter stream flow direction within a straight experimental channel. *Geomorphology*, *44*(1–2), 115–126. https://doi.org/10.1016/S0169-555X(01)00148-9

Beven, K. J. (1979). On the generalized kinematic routing method. *Water Resources Research*, *15*(5), 1238–1242. https://doi.org/10.1029/WR015i005p01238

Beven, K. J., & Carling, P. A. (1992). Velocities, roughness and dispersion in the lowland River Severn. In P. A. Carling, & G. E. Petts (Eds.), *Lowland Floodplain Rivers: Geomorphological Perspectives* (pp. 71–93). Chichester, UK: John Wiley and Sons, Ltd.

Boxall, J., Shepard, W., Guymer, I., & Fox, K. (2003). Changes in water quality parameters due to in-sewer processes. *Water Science and Technology*, *47*(7–8), 343–350. https://doi.org/10.2166/wst.2003.0708

Braudrick, C. A., Dietrich, W. E., Leverich, G. T., & Sklar, L. S. (2009). Experimental evidence for the conditions necessary to sustain meandering in coarse-bedded rivers. *Proceedings of the National Academy of Sciences for the United States of America*, *106*, 16,936–16,941.

Buschmann, M., & Gad-el-Hak, M. (2003). Generalized logarithmic law and its consequences. *The American Institute of Aeronautics and Astronautics*, *41*(1), 40–48. https://doi.org/10.2514/2.1911

Carling, P. A., Cao, Z., Holland, M. J., Irvine, D. A., & Babaeyan-Koupaei, K. (2002). Turbulent flow across a natural compound channel. *Water Resources Research*, *38*(12), 1270. https://doi.org/10.1029/2001WR000902

Chow, V. T. (1959). *Open-channel hydraulics* (pp. 1–280). New York, NY: McGraw-Hill.

Cowan, W. L. (1956). Estimating hydraulic roughness coefficients. *Agricultural Engineering*, *37*, 473–475.

Curran, J. C., & Hession, W. C. (2013). Vegetative impacts on hydraulics and sediment processes across the fluvial system. *Journal of Hydrology*, *505*, 364–376. https://doi.org/10.1016/j.jhydrol.2013.10.013

Darby, S. E. (1999). Effect of riparian vegetation on flow resistance and flood potential. *Journal of Hydraulic Engineering, ASCE*, *125*(5), 443–454. https://doi.org/10.1061/(ASCE)0733-9429(1999)125:5(443)

Davis, P. M., & Atkinson, T. C. (2000). Longitudinal dispersion in natural channels: 3. An aggregated dead zone model applied to the River Severn, UK. *Hydrology and Earth System Sciences*, *4*(3), 373–381. https://doi.org/10.5194/hess-4-373-2000

Davis, P. M., Atkinson, T. C., & Wigley, T. M. L. (2000). Longitudinal dispersion in natural channels: 2. The role of shear flow dispersion and dead zones in the river Severn, UK. *Hydrology and Earth System Sciences*, *4*, 255–371.

Dittrich, A., & Järvelä, J. (2005). Flow-vegetation-sediment interaction. *Water Engineering Research*, *6*, 123–130.

Fathi-Maghadam, M., & Kouwen, M. (1997). Nonrigid, nonsubmerged, vegetative roughness on floodplains. *Journal of Hydraulic Engineering, ASCE*, *123*(1), 51–57. https://doi.org/10.1061/(ASCE)0733-9429(1997)123:1(51)

Ferguson, R. I. (1986). Hydraulics and hydraulic geometry. *Progress in Physical Geography*, *10*(1), 1–31. https://doi.org/10.1177/030913338601000101
Fukuoka, S., & Sayre, W. W. (1973). Longitudinal dispersion in sinuous channels. *Journal of Hydraulics Division, ASCE*, *99*, 195–217.
Ghisalberti, M., & Nepf, H. M. (2005). Mass transport in vegetated shear flows. *Environmental Fluid Mechanics*, *5*, 1–30.
Grathwohl, P. (1998). Diffusion in natural porous media. In *Contaminant transport, sorption/desorption and dissolution kinematics* (pp. 1–207). Kluwer: Academic. https://doi.org/10.1007/978-1-4615-5683-1
Green, H. M., Beven, K. J., Buckley, K., & Young, P. C. (1994). Pollution prediction with uncertainty. In K. J. Beven, P. Chatwin, & J. Millbank (Eds.), *Mixing and transport in the environment* (pp. 1–458). Chichester, UK: John Wiley and Sons, Ltd.
Gurnell, A. M., Bertoldi, W., & Corenblit, D. (2012). Changing river channels: The roles of hydrological processes, plants and pioneer fluvial landforms in humid temperate, mixed load, gravel bed rivers. *Earth-Science Reviews*, *111*(1–2), 129–141. https://doi.org/10.1016/j.earscirev.2011.11.005
Guymer, I., & O'Brien, R. (2000). Longitudinal dispersion due to surcharged manhole. *Journal of Hydraulic Engineering, ASCE*, *126*(2), 137–149. https://doi.org/10.1061/(ASCE)0733-9429(2000)126:2(137)
Hamidifar, H., Omid, M. H., & Keshavarzi, A. (2015). Longitudinal dispersion in waterways with vegetated floodplain. *Ecological Engineering*, *84*, 398–407. https://doi.org/10.1016/j.ecoleng.2015.09.048
Harwood, K., & Brown, A. G. (1993). Fluvial processes in a forested anastomosing river: Flood partitioning and changing flow patterns. *Earth Surface Processes and Landforms*, *18*(8), 741–748. https://doi.org/10.1002/esp.3290180808
Helmio, T. (2004). Flow resistance due to lateral momentum transfer in partially vegetated rivers. *Water Resources Research*, *40*, W05206. https://doi.org/10.1029/2004WR003058
Hoffman, M. R. (2004). Application of a simple space-time averaged porous media model to flow in densely vegetated channels. *Journal of Porous Media*, *73*, 183–191.
Huai, W. X., Zeng, Y. H., Xu, Z. G., & Yang, Z. H. (2009). Three-layer model for vertical velocity distribution in open channel flow with submerged rigid vegetation. *Advances in Water Resources*, *32*(4), 487–492. https://doi.org/10.1016/j.advwatres.2008.11.014
Hui, E.-Q., Hu, X.-E., Jiang, C.-B., Ma, F.-K., & Zhu, Z.-D. (2010). A study of drag coefficient related with vegetation based on the flume experiment. *Journal of Hydrodynamics*, *22*(3), 329–337. https://doi.org/10.1016/S1001-6058(09)60062-7
Ishikawa, Y., Mizuhara, K., & Ashida, S. (2000). Effect of density of trees on drag exerted on trees in river channels. *Journal of Forest Research*, *5*(4), 271–279. https://doi.org/10.1007/BF02767121
Jackson, T. R., Haggerty, R., Apte, V. R., & O'Connor, B. L. (2013). A mean residence time relationship for lateral cavities in gravel-bed rivers and streams: Incorporating streambed roughness and cavity shape. *Water Resources Research*, *49*, 3642–3650. https://doi.org/10.1002/wrcr.20272
Järvelä, J. (2002). Flow resistance of flexible and stiff vegetation: A flume study with natural plants. *Journal of Hydrology*, *269*(1-2), 44–54. https://doi.org/10.1016/S0022-1694(02)00193-2
Järvelä, J. (2004). Determination of flow resistance caused by non-submerged woody vegetation. *International Journal of River Basin Management*, *2*(1), 61–70. https://doi.org/10.1080/15715124.2004.9635222
Jeffries, R., Darby, S. E., & Sear, D. A. (2003). The influence of vegetation and organic debris on flood-plain sediment dynamics: Case study of a low-order stream in the New Forest, England. *Geomorphology*, *51*(1-3), 61–80. https://doi.org/10.1016/S0169-555X(02)00325-2
Kobashi, D., & Mazda, Y. (2005). Tidal flow in riverine-type mangroves. *Wetlands Ecology and Management*, *13*(6), 615–619. https://doi.org/10.1007/s11273-004-3481-4
Kothyari, U. C., Hayashi, K., & Hashimoto, H. (2009). Drag coefficient of unsubmerged rigid vegetation stems in open channel flows. *Journal of Hydraulic Research, ASCE*, *47*(6), 691–699. https://doi.org/10.3826/jhr.2009.3283
Lee, J. K., Roig, L. C., Jenter, H. J., & Visser, H. M. (2004). Drag coefficients for modelling flow through emergent vegetation in the Florida Everglades. *Ecological Engineering*, *22*, 237–248.
Leopold, L. B., & Maddock, T. M. (1953). *The hydraulic geometry of stream channels and some physiographic implications*, *Geological Survey Professional Paper 252* (p. 52). Washington: United States Government Printing Office.
Lewin, J., Ashworth, P. J., & Strick, R. J. P. (2016). Spillage sedimentation on large river floodplains. *Earth Surface Processes and Landforms*, *42*, 290–305.
Li, R. M., & Shen, H. S. (1973). Effect of tall vegetation on flow and sediment. *Journal of Hydraulics Division, ASCE*, No HY5, 793-814.
Li, Y., Wang, Y., Anim, D. O., Tang, C., Du, W., Ni, L., et al. (2013). Flow characteristics in different densities of submerged flexible vegetation from an open-channel flume study of artificial plants. *Geomorphology*, *204*, 314–324. https://doi.org/10.1016/j.geomorph.2013.08.015
Linder, K. (1982). *Der Stromungswiderstand von Pflanzenbeststanden* (p. 75). Braunsweig, Germany: Mitt. Des Leichtweiss Inst. Fuer Wasserbau der TU Braunschweig.
Mazda, Y., Wolanski, E., King, B., Sase, A., Ohtsuka, D., & Magi, M. (1997). Drag force due to vegetation in mangrove swamps. *Mangroves and Salt Marshes*, *1*(3), 193–199. https://doi.org/10.1023/A:1009949411068
Ming, R. H., & Shen, H. W. (1973). Effect of tall vegetations on flow and sediment. *Journal of Hydraulic Research, ASCE*, *99*, 793–814.
Murphy, E., Ghisalberti, M., & Nepf, H. (2007). Model and laboratory study of dispersion in flows with submerged vegetation. *Water Resources Research*, *43*, W05438. https://doi.org/10.1029/2006WR005229
Naot, D., Nezu, I., & Nakagawa, H. (1996a). Unstable patterns in partly vegetated channels. *Journal of Hydraulic Engineering, ASCE*, *122*(11), 671–673. https://doi.org/10.1061/(ASCE)0733-9429(1996)122:11(671)
Naot, D., Nezu, I., & Nakagawa, H. (1996b). Hydrodynamic behaviour of partly vegetated open channels. *Journal of Hydraulic Engineering, ASCE*, *122*(11), 625–633. https://doi.org/10.1061/(ASCE)0733-9429(1996)122:11(625)
Nepf, H. M. (1999a). Flow and transport in regions with aquatic vegetation. *Annual Review of Fluid Mechanics*, *44*, 123–142.
Nepf, H. M. (1999b). Drag, turbulence, and diffusion in flow through emergent vegetation. *Water Resources Research*, *35*(2), 479–489. https://doi.org/10.1029/1998WR900069
Nepf, H. M., Mugnier, C. G., & Zavistoski, R. A. (1997). The effects of vegetation on longitudinal dispersion. *Estuarine, Coastal and Shelf Science*, *44*(6), 675–684. https://doi.org/10.1006/ecss.1996.0169
Nicholas, A. P., & Walling, D. E. (1998). Numerical modelling of flood-plain hydraulics and suspended sediment transport and deposition. *Hydrological Processes*, *12*(8), 1339–1355. https://doi.org/10.1002/(SICI)1099-1085(19980630)12:8<1339::AID-HYP618>3.0.CO;2-6
Pasche, E., & Rouvé, G. (1985). Overbank flow with vegetatively roughened flood plains. *Journal of Hydraulic Engineering, ASCE*, *111*(9), 1262–1278. https://doi.org/10.1061/(ASCE)0733-9429(1985)111:9(1262)
Paudel, R., Grace, K. A., Galloway, S., Zamorano, M., & Jawitz, J. W. (2013). Effects of hydraulic resistance by vegetation on stage dynamics of a stormwater treatment wetland. *Journal of Hydrology*, *484*, 74–85. https://doi.org/10.1016/j.jhydrol.2013.01.031

Pedregal, D. J., Taylor, C. J., & Young, P. C. (2007). *System identification, time series analysis and forecasting. The Captain Toolbox. Handbook V2.0 February 2007, Centre for Research on Environmental Systems and Statistics (CRES)* (p. 273). Lancaster, UK: Lancaster University.

Perucca, E., Camporeale, C., & Ridolfi, L. (2009). Estimation of the dispersion coefficient in rivers with riparian vegetation. *Advances in Water Resources*, *32*(1), 78–87. https://doi.org/10.1016/j.advwatres.2008.10.007

Piégay, H., Citterio, A., & Astrade, L. (1998). Interactions between large woody debris and meander cut-off [example of the Mollon reach on the Ain River, France]. *Zeitschrift für Geomorphologie*, *42*, 187–208. [In French]

Raudkivi, A. J. (1967). *Loose boundary hydraulics* (p. 331). Oxford, UK: Pergamon Press.

Rhee, D. S., Woo, H., Kwon, B. A., & Ahn, H. K. (2008). Hydraulic resistance of some selected vegetation in open channel flows. *River Research and Applications*, *24*(5), 673–687. https://doi.org/10.1002/rra.1143

Richardson, K., & Carling, P. A. (2006). The hydraulics of a straight bedrock channel: Insights from solute dispersion studies. *Geomorphology*, *82*(1-2), 98–125. https://doi.org/10.1016/j.geomorph.2005.09.022

Righetti, M. (2008). Flow analysis in a channel with flexible vegetation using double averaging method. *Acta Geophysica*, *56*(3), 801–823. https://doi.org/10.2478/s11600-008-0032-z

Righetti, M., & Armanini, A. (2002). Flow resistance in open channel flows with sparsely distributed bushes. *Journal of Hydrology*, *269*(1-2), 55–64. https://doi.org/10.1016/S0022-1694(02)00194-4

Rutherford, J. C. (1994). *River mixing* (p. 347). Chichester, UK: John Wiley and Sons, Ltd.

Schoneboom, T., Aberle, J., & Dittrich, A. (2011). Spatial variability, mean drag forces, and drag coefficients in an array of rigid cylinders. In P. Rowinski (Ed.), *Experimental methods in hydraulic research (GeoPlanet: Earth and planetary sciences)* (Vol. 1, pp. 255–265). Berlin: Springer.

Serra, T., Fernando, H. J. S., & Rodriguez, R. V. (2004). Effects of emergent vegetation on lateral diffusion in wetlands. *Water Research*, *38*(1), 139–147. https://doi.org/10.1016/j.watres.2003.09.009

Shucksmith, J. D., Boxall, J. B., & Guymer, I. (2011). Determining longitudinal dispersion coefficients for submerged vegetated flow. *Water Resources Research*, *47*, W10516. https://doi.org/10.1029/2011WR010547

Smart, P. L., & Laidlaw, I. M. S. (1977). An evaluation of some fluorescence dyes for water tracing. *Water Resources Research*, *13*(1), 15–33. https://doi.org/10.1029/WR013i001p00015

Soulitis, D., & Prinos, P. (2008). Turbulence in vegetated flows: Volume-averaging analysis and modelling aspects. *Acta Geophysica*, *56*(3), 894–917. https://doi.org/10.2478/s11600-008-0027-9

Stoesser, T., Kim, S. J., & Diplas, P. (2010). Turbulent flow through idealized emergent vegetation. *Journal of Hydraulic Engineering, ASCE*, *136*(12), 1003–1017. https://doi.org/10.1061/(ASCE)HY.1943-7900.0000153

Straatsma, M. W., van der Perk, M., Schipper, A. M., de Nooij, R. J. W., Leuven, R. S. E. W., Huthoff, F., & Middelkoop, H. (2013). Uncertainty in hydromorphological and ecological modelling of lowland river floodplains resulting from land cover classification errors. *Environmental Modelling and Software*, *42*, 17–29. https://doi.org/10.1016/j.envsoft.2012.11.014

Tal, M., & Paola, C. (2007). Dynamic single-thread channels maintained by the interaction of flow and vegetation. *Geology*, *35*(4), 347–350. https://doi.org/10.1130/G23260A.1

Tanino, Y., & Nepf, H. M. (2008). Laboratory investigation of mean drag in a random array of rigid, emergent cylinders. *Journal of Hydraulic Engineering, ASCE*, *134*(1), 34–41. https://doi.org/10.1061/(ASCE)0733-9429(2008)134:1(34)

Tealdi, S., Camporeale, C., Perucca, E., & Ridolfi, L. (2010). Longitudinal dispersion in vegetated rivers with stochastic flows. *Advances in Water Resources*, *33*(5), 562–571. https://doi.org/10.1016/j.advwatres.2010.03.003

Temple, D. M., Robinson, K. M., Ahring, R. M., & Davis, A. G. (1987). Stability design of grass-lined open channels. In *Agriculture handbook 667*, *Agricultural Research Service* (pp. 1–167). Washington, DC: U.S. Department of Agriculture.

Valentine, E. M., & Wood, I. R. (1977). Longitudinal dispersion with dead zones. *Journal of Hydraulics Division, ASCE*, *103*, 975–990.

van Dijk, W. M., Teske, R., van de Lageweg, W. I., & Kleinhans, M. G. (2013). Effects of vegetation distribution on experimental river channel dynamics. *Water Resources Research*, *49*, 7558–7574. https://doi.org/10.1002/2013WR013574

van Rijn, L. C. (1984). Sediment transport. Part III: Bed forms and alluvial roughness. *Journal of Hydraulic Engineering*, *110*, 1733–1754.

Västilä, K., Järvelä, J., & Koivusalo, H. (2016). Flow–vegetation–sediment interaction in a cohesive compound channel. *Journal of Hydraulic Engineering*, *142*(1), 04015034. https://doi.org/10.1061/(ASCE)HY.1943-7900.0001058

Wallis, S. G. (1994). Simulation of solute transport in open channel flow. In K. J. Beven, P. Chatwin, & J. Millbank (Eds.), *Mixing and transport in the environment* (pp. 89–112). Chichester, UK: John Wiley and Sons, Ltd.

Wallis, S. G., Guymer, I., & Bilgi, A. (1990). A practical engineering approach to modelling longitudinal dispersion. In R. A. Falconer, P. Goodwin, & R. G. S. Matthew (Eds.), *Hydraulic and environmental modelling of coastal, estuarine and river waters* (pp. 291–300). London: Gower Technical.

Wallis, S. G., Young, P. C., & Beven, K. J. (1989). Experimental investigation of the aggregated dead zone model for longitudinal solute transport in stream channels. *Proceedings of the Institution of Civil Engineers*, *87*, 1–22.

Wolanski, E., Jones, M., & Bunt, J. S. (1980). Hydrodynamics of a tidal creek-mangrove swamp system. *Australian Journal of Marine and Freshwater Research*, *31*(4), 431–450. https://doi.org/10.1071/MF9800431

Wu, F.-C., Shen, H. W., & Chou, Y.-J. (1999). Variation of roughness coefficients for unsubmerged and submerged vegetation. *Journal of Hydraulic Engineering, ASCE*, *125*(9), 934–942. https://doi.org/10.1061/(ASCE)0733-9429(1999)125:9(934)

Yalin, M. S. (1977). *Mechanics of sediment transport* (2nd ed.). Oxford, NY: Pergamon Press.